基礎研究の新たな方向性を解く37

疾患解明Overviewy

内耳性難聴：新しい治療法開発への展望

中川隆之・喜多由紀・伊藤壽一

疾患の概要

感音難聴は，最も頻度の高い身体障害であり，感音難聴の多くは内耳の蝸牛障害に起因し，内耳性難聴とよばれる．哺乳類の場合，内耳の感覚細胞である有毛細胞や一次ニューロンである神経節細胞は再生能力に乏しい．したがって，これらの細胞が障害を受けると難聴は恒久的なものとなる．発生学や分子生物学的な知見を利用して，これらの細胞を再生させようという試みが進められている．

はじめに

感音難聴は，最も頻度の高い身体障害の1つとされている．感音難聴は，空気の疎密波である音響刺激の中枢までの伝達経路のうち，蝸牛以降の過程が障害されたものを示すが，その多くは，内耳の蝸牛障害に起因し，内耳障害による感音難聴は内耳性難聴とよばれる．

内耳性難聴の原因としては，音響外傷，耳毒性薬物，遺伝子異常，老化などがある．聾（ろう）もしくは高度難聴は新生児の1,000人に1人認められ，2,000人に1人は成人するまでに発症する．70歳を超えた人口の6割には，高度感音難聴が存在する．このような高い有病率にもかかわらず，症状が固定した慢性期の内耳性難聴に関して現在臨床で使える治療法は補聴器と人工内耳に限られている．1980年代に導入された人工内耳は，刺激電極を蝸牛に挿入し，直接ラセン神経節を刺激する治療法であり，多くの高度難聴者にとって，聴覚を獲得することができる医療として完全に定着している．しかし，これらの治療法は対症療法でしかなく，また，失われた聴力を完全に補償するものではない．

このような背景から，内耳性難聴を克服すべく，多くの基礎的研究が展開されている．本稿では，新しい治療法の開発という視点から，最近の知見および研究の方向性について，①内耳発生に関する分子生物学的研究成果を応用し，成熟した内耳に残存している再生能力を誘導する，②再生能力が乏しい哺乳類内耳に再生能力がある細胞を外部から導入する（細胞移植），といった内容を中心に述べる（概念図）．

遺伝子・分子レベルでの知見

音響刺激は，空気の疎密波として，鼓膜を振動させる．鼓膜の振動は，中耳にある3つの耳小骨を介して蝸牛に伝えられる．耳小骨の振動は，蝸牛の感覚上皮（コルチ器）を振動させ，感覚上皮の感覚細胞（有毛細胞）が振動エネルギーを神経信号に変換し，蝸牛軸に存在する蝸牛の一次神経節であるラセン神経節細胞を興奮させ，音響刺激は中枢に伝達される（図）．

近年，先天性難聴のみならず，多くの内耳性難聴に

Novel strategies for the treatment of sensorineural hearing loss

Takayuki Nakagawa/Yayoi S. Kikkawa/Juichi Ito：Department of Otolaryngology, Head and Neck Surgery, Graduate School of Medicine, Kyoto University（京都大学大学院医学研究科耳鼻咽喉科頭頸部外科）

●概念図● 内耳再生へのストラテジー

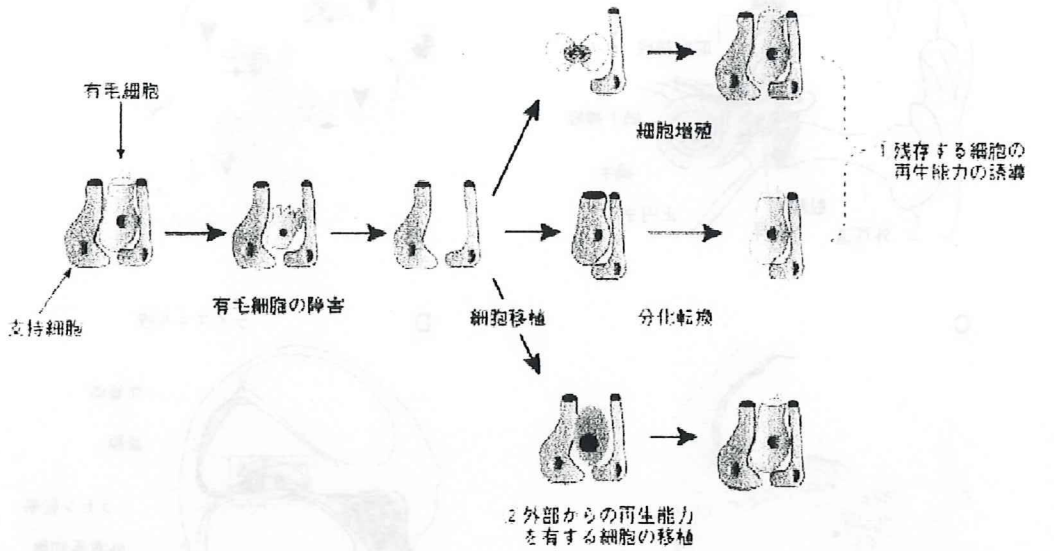

感覚上皮における有毛細胞再生へのストラテジーを示す．内在する再生能力を誘導する方法として，1 残存する支持細胞の増殖を誘導し，増殖した支持細胞を有毛細胞に分化させる．あるいは残存する支持細胞を直接有毛細胞へ分化転換する方法が挙げられる．有毛細胞の再生には 2 外部から再生能力を有する細胞を内耳に移植する方法（細胞移植）も考えられる．

は遺伝子異常が関与していることが明らかにされつつある．難聴家系調査やゲノムプロジェクト，突然変異マウスなどの研究により，多くの難聴にかかわる遺伝子がこれまでに判明している．代表的なものを表に示す．また，インターネット上に難聴遺伝子データベースが公開されており，新しいデータが逐次報告されている（http://webhost.ua.ac.be/hhh/）．これらには転写因子や分子モーター，ギャップジャンクションタンパク質，イオンチャネルタンパク質，細胞外マトリクス分子など多種の遺伝子が含まれており，このような多数の難聴遺伝子の存在は，それだけ内耳の発生，機能が複雑に制御されていることを示している．こうした原因遺伝子を同定し，そのタンパク質の機能を解析することは，該当する遺伝性難聴の治療法の開発や遺伝子スクリーニングなど臨床面においても重要であるが，内耳発生，特に聴覚に関連する細胞の発生，分化機構を解明する点でも重要な意味をもつ．

近年の内耳発生に関する研究成果のなかで，ノッチ情報伝達系に関する知見は，内耳有毛細胞再生へ新しい手がかりを提供した画期的なものといえる[1]．内耳感覚上皮の発達過程において，1 列の内有毛細胞，3 列の外有毛細胞，分化した支持細胞など，蝸牛の複雑な細胞構成の構築にはノッチ情報伝達系による側方抑制が機能していることが，ノッチ情報伝達系のリガンドや関連する転写因子のノックアウトマウスの解析により示されている．ノッチ受容体は隣接細胞が発現するリガンドが結合するとγセクレターゼ活性により細胞膜内領域で切断され，その細胞内領域が核内に移行し，核内の transactivator である RBP-J と結合し，標的遺伝子の転写を開始する．Cre-loxP システムを利用した RBP-J 遺伝子のコンディショナルノックアウトマウスの系では，外有毛細胞の外側，つまり通常は支持細胞の存在する領域に，有毛細胞が認められ[2]，ノッチ情報伝達系が遮断されることにより，支

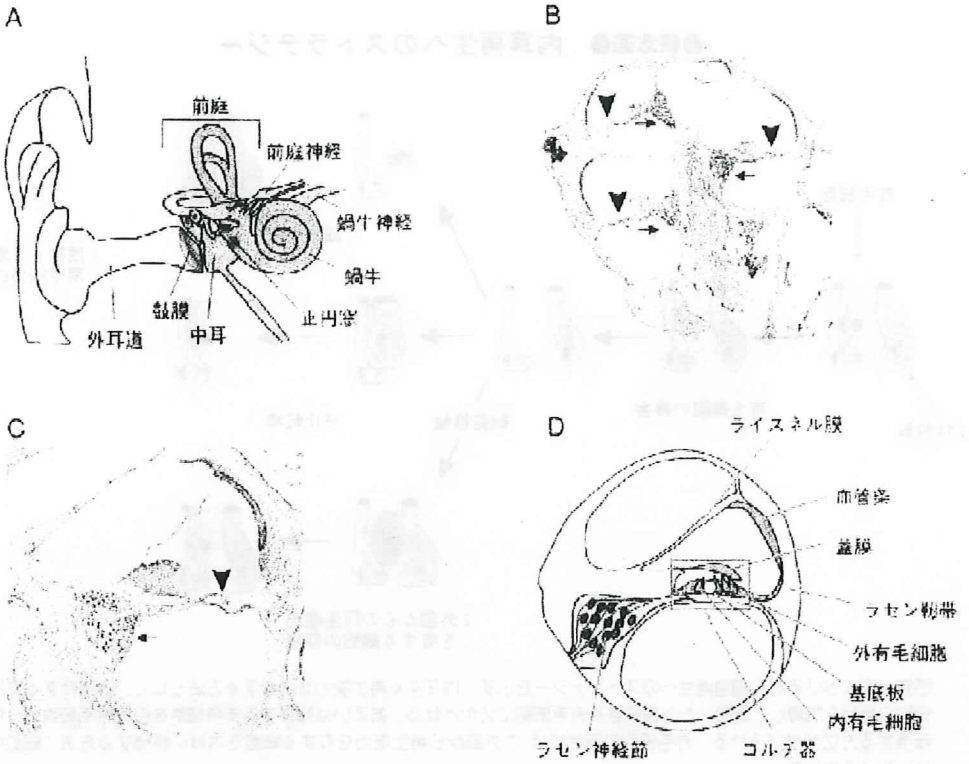

図　内耳，蝸牛の解剖

A）音源は外耳道を通り，鼓膜を振動させ，中耳に存在する耳小骨を振動させる．耳小骨の振動は内耳にある蝸牛に伝達される．

B，C）マウス蝸牛断面図．蝸牛軸にそってラセン神経節（矢印）が存在する．矢頭は感覚上皮（コルチ器）の位置を示す．

D）蝸牛断面模式図

持細胞が有毛細胞に分化することが示されている．

内耳発生段階における細胞周期制御機構に関連する一連の報告も，内耳再生に多くの示唆を与えるものといえる．発達段階のマウス内耳感覚上皮予定領域では，胎生期13日前後で細胞増殖が停止し，急速に有毛細胞，支持細胞の分化が誘導される．つまり，この時期の前後で発現変化の認められる細胞増殖に関連する因子が細胞増殖の停止に関連することが推察される．サイクリン依存性キナーゼ阻害タンパク質の1つである$p27^{Kip1}$がこの時期の感覚上皮予定領域の細胞増殖が停止に重要な役割を果たしていることが明らかにされ，$p27^{Kip1}$をノックアウトしたマウスでは過剰に有毛細胞が出現し，生後も細胞増殖が認められることが示された[7]．内耳感覚上皮の細胞増殖制御については，RBP/E2F系などいくつかの因子が関与していることが示されているが，$p27^{Kip1}$は支持細胞に比較的特異的に発現することから，支持細胞の増殖誘導について鍵を握る因子と考えられている．

内耳再生への試み①：内在する細胞による再生

鳥類では，哺乳類と異なり，内耳有毛細胞が再生することが知られているが，そのメカニズムとして1）支持細胞の増殖，分化による再生と2）残存する支持細胞が有毛細胞に分化転換する，2つの経路があることが知られている[8]．哺乳類でも，標的となる分子を操作することにより，同様のストラテジーで再生を誘導できる可能性がある．

前述したノッチ情報伝達系の転写因子を過剰発現することにより，生後の成熟した哺乳類蝸牛感覚上皮で

表　難聴遺伝子

分子名	ヒト遺伝子名	遺伝性難聴の種類	変異マウス	タンパク質の機能
Pou4f3（Brn3c）	POU4F3	DFNA15		転写因子
Pax3	PAX3	Waardenburg症候群 type Ⅰ，Ⅲ	Splotch	転写因子
Myosin Ⅶa	MYO Ⅶa	Usher症候群1B DFNB2 DFNA11	Shaker-1	分子モーター
Myosin XV	MYO XV	DFNB3	Shaker-2	分子モーター
Connexin26	GJB2（CX26）	DFNA3		ギャップジャンクション タンパク質
Claudin14	CLDN14 (Claudin14)	DNFB29		タイトジャンクション タンパク質
KCNQ4 (potassium channel)	KCNQ4	DFNA2		チャネルタンパク質
Cadherin23	CDH23	Usher症候群1D	Waltzer	細胞膜接着因子
Protocadherin15	PCDH15	Usher症候群1F	Ames waltzer	細胞膜接着因子
Usherin	Usherin	Usher症候群2A		細胞膜接着因子
Alpha-tectorin		DFNA8 DFNA12 DFNB21		蓋膜構成タンパク質
Collagen	COL4A5	Alport症候群		細胞外マトリクス分子

代表的な難聴遺伝子と遺伝性難聴の種類，変異マウス，遺伝子がコードするタンパク質の機能を示す

も支持細胞から有毛細胞への分化転換誘導が可能であることが示された．ミシガン大学のRaphaelのグループは，成体モルモットの蝸牛感覚上皮にノッチ情報伝達系の転写因子である*Atho1*をアデノウイルスを用いて過剰発現させることにより，支持細胞から有毛細胞への分化転換が起こりうることを示し[5]，アミノ配糖体で聾としたモルモットでも同様の操作により，残存する支持細胞から有毛細胞への分化転換誘導が可能であることを示した[6]．一方，山本ら[2]は，ノッチ情報伝達系の遮断により，内耳感覚上皮でのAtoh1発現が亢進し，支持細胞から有毛細胞への分化転換が起こりうることを器官培養系の実験で示した．そこでわれわれは，Raphaelらのグループが用いたモルモット障害モデルを使用し，薬物の内耳局所投与によるノッチ情報伝達系阻害による支持細胞から有毛細胞への分化転換について調べた．ノッチ情報伝達系阻害薬としては，山本らが培養系で有効性を確認したγセクレターゼ阻害剤であるMDL28170を用いた．結果，支持細胞から有毛細胞への分化転換を示唆する所見が認められた[7]．障害後に認められた新生有毛細胞の数は，ウイルスベクターによるAtoh1過剰発現に比較すると少なく，また新生有毛細胞が認められる部位も限定されていた．しかしながら，アデノウイルスベクターによる内耳への遺伝子導入という手法に比べ，内耳への薬物局所投与という方法は，臨床応用に近い手法といえ，ノッチ情報伝達系の操作による内耳有毛細胞再生を臨床応用するという観点からは，大きな前進といえる．近年，特定のタンパク質の機能制御を行う小分子化合物を用いた研究（chemical genetics）が注目を集めており，今後，遺伝子操作で得られた研究成果を「内耳への薬物投与」に置き換えることにより，臨床応用への可能性を高める工夫が積極的になされるであろう．

鳥類での内耳有毛細胞再生のメカニズムを哺乳類に応用するという観点から，哺乳類での支持細胞の増殖誘導も重要な研究アプローチといえる．支持細胞の増殖停止機構として，細胞周期を抑制するサイクリン依存性キナーゼ阻害タンパク質である$p27^{Kip1}$の役割が最も注目されている．生後の蝸牛感覚上皮においても支持細胞の$p27^{Kip1}$の発現を抑制することができれば，支

持細胞が再び分裂，増殖する可能性がある．$p27^{Kip1}$の発現制御メカニズムとしては，$p27^{Kip1}$遺伝子からの転写，翻訳レベルと$p27^{Kip1}$タンパク質の細胞内での分解レベルの２つがある．後者のメカニズムにかかわるのが，Ｆボックスタンパク質の１つであるskp2である．skp2は$p27^{Kip1}$のユビキチン化に関与し，skp2などの働きでユビキチンを付加された$p27^{Kip1}$はプロテアソームにて分解される．

発達段階に応じてマウス内耳感覚上皮でのskp2の発現変化を組織学的に解析することで，内耳感覚上皮で細胞増殖が活発な時期には，skp2により$p27^{Kip1}$の発現が抑制されており，内耳感覚上皮で有毛細胞，支持細胞への分化運命が決定されるタイミングにおいては，$p27^{Kip1}$の発現は支持細胞のみに限定され，有毛細胞では消失することが明らかになった．この有毛細胞でのp27の発現の消失にskp2は関与せず[8]，遺伝子からの転写レベルよりも上流で$p27^{Kip1}$の発現が制御されている．したがって，成熟した内耳感覚上皮支持細胞でのp27発現抑制には，skp2過剰発現によるタンパク質分解の促進もしくはRNA干渉による翻訳の抑制が有効な手段と推察される．養田らは，ウイルスベクターを用いたskp2の内耳感覚上皮での過剰発現が細胞増殖を誘導すると報告している[9]．しかし，細胞周期にリエントリーすることは，細胞死の誘導につながる可能性もあり[10]，今後の検討が注目される．

内耳再生への試み2）細胞移植

哺乳類内耳の再生能力が限られているのならば，再生能力のある細胞を内耳に送り込んでやればよいのではないか，という発想で内耳への細胞移植実験は開始された．最初の内耳への細胞移植実験は，内耳と同じ外胚葉系の幹細胞である神経幹細胞を用いたものである．有毛細胞障害を惹起した内耳に神経幹細胞を移植すると，内耳組織内に移植細胞の侵入を示唆する所見が認められた．また，ごく限られてはいるが，前庭感覚上皮内に侵入した移植細胞の一部が内耳有毛細胞のマーカーであるミオシン7aを発現している所見が認められた[11]．この結果は，神経幹細胞は障害を受けた内耳感覚上皮には侵入できるということを示しており，有毛細胞に分化する可能性があることを呈示するものとして内外の注目を集めた．内耳組織由来の細胞や胚性幹細胞由来の細胞移植でも，感覚上皮内に移植細胞が侵入し，有毛細胞様の細胞に分化することが報告されているが，機能再生に関連する報告はなされていない．いかに，有毛細胞や支持細胞といった感覚上皮特有の細胞に効率よく分化する細胞を開発するか，また，移植した細胞をいかにして感覚上皮内へと誘導するかが，解決すべき問題点として残されている．

細胞移植による内耳再生研究では，ラセン神経節細胞が主な研究対象とされている．現在，高度難聴に対する唯一の治療法は人工内耳であるが，人工内耳を埋め込んでもラセン神経節細胞に障害がある場合，良好な聞き取りは得られない．細胞移植によって，ラセン神経節細胞が再生すれば，人工内耳での聞き取りも向上すると期待される．このような臨床的背景に加え，神経細胞は種々の細胞から比較的分化誘導しやすいことにより，細胞移植によるラセン神経節細胞再生に関する研究が活発に行われている．種々の細胞が移植細胞のソースとして用いられているが，最も神経細胞の再生能力が高い細胞が胚性幹細胞（ES細胞）といえる．ES細胞では，高率に神経細胞へと分化誘導する方法が確立されており，*in vitro*, *in vivo*での移植実験がいくつか行われている．最も注目すべき点としては，*in vivo*の移植実験で機能回復を示唆する所見が認められているという点である．

神経細胞へ分化誘導したマウスES細胞を，ラセン神経節変性をあらかじめ誘導したモルモットに移植し，４週間後に，電気刺激聴性脳幹反応にて機能評価したところ，コントロールとしたシャムオペ（偽手術）群よりも有意に機能が回復していることが認められた[12]．組織学的にも，移植細胞由来神経細胞の蝸牛軸での局在が確認されている．今後，移植細胞由来神経細胞が直接的に機能回復に寄与しているのか，栄養因子の供給などの間接的な効果なのかを検討する必要がある．

臨床応用への展望

第一に内耳に内在する細胞を活性化し，内耳の再生を誘導し，内耳性難聴の治療に応用する試みについては，内耳再生を妨げている因子を抑制し，再生を誘導する方法が最も臨床に近い方法といえる．しかしながら，この方法による機能回復に関する知見は，報告されておらず，今後の課題といえる．

細胞移植による内耳再生では，人工内耳とも深いかかわりをもつラセン神経節細胞の再生が最も臨床応用に近い位置にある．すでに霊長類での実験が開始されている．最大の問題は，移植細胞ソースにかかわる倫理的な面といえる．ES細胞は他の幹細胞に比べて，均一な性質をもつ細胞を大量に準備することが可能であり，ラセン神経節細胞再生に関しても現在のところ最も能力の高い細胞といえる．しかし，わが国では，ヒトES細胞を使用した研究承認へのハードルはきわめて高い．このような背景から，ES細胞をソースとした研究で得られた成果を他の自己由来細胞で実現しようとする方向性が模索されている．最近，線維芽細胞からES細胞と同様の性質をもった細胞をつくることが可能であることも報告されており[13]，自己由来細胞からES細胞様の細胞をつくることが可能となれば，大きく展開は変わる可能性がある．

文献

1）Kelly, M. W.：Int. J. Dev. Biol., 51：571-583, 2007
2）Yamamoto, N. et al.：J. Mol. Med., 84：37-45, 2006
3）Lowenheim, H. et al.：Proc. Natl. Acad. Sci. USA, 96：4084-4088, 1999
4）Stone, J. S. & Cotanche, D. A.：Int. J. Dev. Biol., 51：633-647, 2007
5）Kawamoto, K. et al.：J. Neurosci., 23：4395-4400, 2003
6）Izumikawa, M. et al.：Nature Med., 11：271-276, 2005
7）Hori, R. et al.：Neuroreport, in press (2007)
8）Dong, Y. et al.：Neuroreport, 14：759-761, 2003
9）Minoda, R. et al.：Hear. Res., 232：44-51, 2007
10）Laine, H. et al.：J. Neurosci., 27：1434-1444, 2007
11）Tateya, I. et al.：Neuroreport, 14：1677-1681, 2003
12）Okano, T. et al.：Neuroreport, 16：1919-1922, 2005
13）Takahashi, K. et al.：Cell, 126：663-676, 2006

参考図書

『Development of the Inner Ear』Kelley, M. W. et al., Springer, 2005

『ここまで進んだ幹細胞研究と再生医療2006』（田賀哲也，中畑龍俊／編），実験医学増刊号，Vol.24 No.2，羊土社，2006

『中枢神経の機能再生―細胞治療と人工臓器―』，Medical Bio，オーム社，2007年7月号

筆頭著者プロフィール

中川隆之：1989年大阪市立大学医学部卒業，'95年同大学院医学研究科修了，内耳のアポトーシス研究を行い，医学博士取得．2001年より京都大学大学院医学研究科耳鼻咽喉科頭頸部外科助教．現在，内耳再生，特に新しい感音難聴治療方法の開発を目的として研究を行っている．

The potential use of bone marrow stromal cells for cochlear cell therapy

Sadia Sharif[a,c], Takayuki Nakagawa[a], Tsunehisa Ohno[a], Masahiro Matsumoto[a], Tomoko Kita[a,b], Sheikh Riazuddin[c] and Juichi Ito[a]

[a]Department of Otolaryngology-Head and Neck Surgery, Kyoto University Graduate School of Medicine, [b]Organogenesis and Neurogenesis Group, Center for Developmental Biology, RIKEN, Kobe, Japan and [c]National Center of Excellence in Molecular Biology, University of the Punjab, Pakistan

Correspondence to Dr Takayuki Nakagawa, MD, PhD, Department of Otolaryngology-Head and Neck Surgery, Graduate School of Medicine, Kyoto University, Kawaharacho 54, Shogoin, Sakyo-ku, 606-8507 Kyoto, Japan
Tel: +81 75 751 3346; fax: +81 75 751 7225; e-mail: tnakagawa@ent.kuhp.kyoto-u.ac.jp

Received 10 October 2006; accepted 25 November 2006

This study investigated the potential of bone-marrow stromal cell transplantation for cell replacement therapy in the cochlea. Bone-marrow stromal cells labeled with enhanced green fluorescent protein were injected into the perilymphatic space of normal cochleae in mice. Histological analysis 2 weeks after transplantation demonstrated that transplanted cells settled within the cochlear tissues, especially in the spiral ligament and the spiral limbus, although most transplants were located in the perilymphatic space. Some of the transplanted cells expressed the cochlear gap-junction protein connexin 26. These findings indicate the potential of bone-marrow stromal cells for delivering therapeutic molecules and for the restoration of cochlear cells, particularly in the spiral ligament and the spiral limbus. *NeuroReport* 18:351–354

Keywords: bone-marrow stromal cell, cell therapy, cochlea, migration, transplantation

Introduction

Treatment options for sensorineural hearing loss (SNHL) are currently limited to cochlear implants and hearing aids. Hence, there is a requirement for alternative means of biological therapy, including cell and/or gene therapy. Indeed, recent studies have indicated that cell or gene therapy could be utilized to regenerate hair cells [1,2] and neurons [3] in the inner ear, and to deliver therapeutic molecules to the inner ear [4–6]. More recently, transplantation of gene-transfected cells has been reported as an efficient strategy to deliver genes into the inner ear [7].

Bone-marrow stromal cells (BMSCs) are possible candidates for transplants for cell therapy for the treatment of SNHL. They have the potential for differentiation into various types of cells and are easily obtained from one's own bone marrow. In addition, BMSCs are capable of secretion of several growth factors [8], which are included in cochlear protectants [9–11]. BMSC transplantation, therefore, could be utilized in three different strategies for inner ear treatment, restoration of missing cells, providing growth factors and delivering genes. In this study, we examined the distribution and characteristics of BMSCs after transplantation into cochleae of C57BL/6 mice to evaluate the potential of BMSCs as a source of cells for cell-replacement-therapy for the cochlea.

Materials and methods

Animals

Male C57BL/6 mice (n=6, SLC Japan, Hamamatsu, Japan) aged 10 weeks were used as the recipients. The experimental protocols were approved by the Animal Research Committee of Kyoto University Graduate School of Medicine, and were conducted in accordance with the US National Institutes of Health Guidelines for the Care and Use of Laboratory Animals.

Bone-marrow stromal cells

The BMSCs were obtained from enhanced green fluorescent protein (GFP)-transgenic mice [strain B6;C3-*Tg(ACtb-EGFP)CX-FM139Osb*] [12]. Under general anesthesia with ketamine (75 mg/kg) and xylazine (9 mg/kg), the tibias and femurs of the animals (n=4) were collected, and the medullary cavity was aspirated to harvest the bone marrow. The BMSCs were cultured in a 25-cm^2 flask with 8 ml of Iscove's modified Dulbecco's medium (Invitrogen, Carlsbad, California, USA) supplemented with 20% fetal bovine serum (Thermo Trace, Victoria, Australia), 100 U/ml of penicillin (Nacalai Tesque Inc., Kyoto, Japan) and 100 µg/ml of streptomycin (Nacalai Tesque Inc.). The cells were cultured at 37°C under 5% CO_2. The medium was changed twice weekly until the cells were 80% confluent. Non-adherent cells were removed during the medium-change procedure and the adherent cells were collected. After two passages, the cells were suspended in Iscove's modified Dulbecco's medium at a concentration of 1×10^5 cells/µl.

Transplantation

Cell transplantation was performed under general anesthesia with ketamine and xylazine. A retroauricular incision was made in the left ear of each mouse and the otic bulla

was exposed. The bony wall of the bulla was partially resected to expose the basal turn of each cochlea. A small perforation was then made in the lateral wall at the basal turn of the cochlea corresponding to the location of the scala tympani (ST). Cell suspensions of GFP-labeled BMSCs (2 μl; 10^5 cells/μl) were injected through a fine glass needle using a microinfusion pump. Subsequently, the perforation was plugged with a fat graft and covered with fibrin glue.

Histology

Under general anesthesia, the animals were transcardially perfused with phosphate-buffered saline at pH 7.4, followed by 4% paraformaldehyde in phosphate buffer at pH 7.4 on day 14. The temporal bones were immediately dissected out and immersed in the same fixative for 4 h at 4°C. After decalcification, cryostat sections (8 μm thickness) were cut and immunohistochemical analysis for GFP, CD43, nestin, β-III-tubulin, E-cadherin and Cx26 was performed. BMSCs grown on sterile cover glasses were also subjected to immunocytochemical analysis to determine the characteristics of the BMSCs before transplantation. Anti-GFP mouse monoclonal (1:200; Invitrogen, San Diego, California, USA) or rabbit polyclonal (1:500, Molecular probes, Eugene, Oregon, USA), anti-CD43 rat monoclonal (1:200; Pharmingen, San Diego, California, USA), anti-nestin rat monoclonal (1:200; Pharmingen), anti-β-III-tubulin mouse monoclonal (1:500, Covance Research Products, Berkeley, California, USA), anti-Cx26 rabbit polyclonal (1:500; Zymed, San Francisco, California, USA) and anti-E-cadherin mouse monoclonal antibody (1:200; Takara Bio, Otsu, Japan) were used as the primary antibodies. The secondary antibody was Alexa-546 or 488-conjugated anti-mouse, rat or rabbit antibody (1:400; Molecular Probes). Counterstaining by 4′,6-diamidino,2-phenylindole dihydrochloride (DAPI; 1 μg/ml in phosphate-buffered saline; Molecular Probes) was performed at the end of the staining procedures. Specimens stained without primary antibodies served as negative controls. Cryostat-sections of mouse cerebellum on embryonic day 12 were used as positive controls for nestin. The specimens were viewed with a Nikon Eclipse E600 fluorescence microscope (Nikon, Tokyo, Japan) or a Leica TCS-SP2 confocal laser-scanning microscope (Leica Microsystems, Tokyo, Japan).

Four mid-modiolar sections were chosen from each cochlea and subjected to quantitative analysis of the number of transplanted cells in the cochlea. We counted the number of cells expressing both GFP and DAPI as transplant-derived cells. The distribution of the engrafted cells was divided into four compartments: the scala vestibuli (SV), the scala media, the ST and the cochlear tissues. In addition, the cochlear tissues were further subdivided into three compartments: the spiral ligament (SL), the spiral limb (SLB) and the other components of the cochleae. The number of transplant-derived cells expressing CD34, nestin or Cx26 was also counted in four sections from each cochlea. The expression ratio for each marker was then determined by dividing the numbers of transplant-derived cells expressing each marker by those of transplant-derived cells in each section. The average in four sections was defined as the data for the cochlea. The expression ratios for these markers were also calculated using four samples of BMSCs grown on sterile cover glasses. All the data were represented by the means and the standard deviations.

Statistics

Statistical analyses for the location of BMSC-derived cells in the cochlea were performed using one-way analysis of variance followed by the Scheffe's test. The unpaired *t*-test was used in analyses of the expression ratios for CD34, nestin and Cx26. A P value <0.05 was considered statistically significant.

Results

BMSC-derived cells labeled with GFP were found in all the transplanted cochleae (Fig. 1a). The mean number of GFP-positive cells in one mid-modiolar section per cochlea was 180 ± 38 ($n=6$). The transplanted cells were distributed from the base to the apex of the cochleae. No apparent difference in distribution of transplanted cells was found among the turns of cochleae. BMSC-derived cells were predominantly located in the perilymphatic space of the cochleae: $67.3 \pm 7.3\%$ in the ST and $18.1 \pm 10.8\%$ in the SV (Fig. 1b). The ST was the region in which BMSC-derived cells were most frequently observed. BMSC-derived cells were also observed within the cochlear tissues ($12.8 \pm 9.2\%$), indicating the migration activity of BMSCs into various parts of the cochleae. Of BMSC-derived cells located in cochlear tissues, $57.4 \pm 8.0\%$ were found in the SL (Fig. 1b–d) and $17.3 \pm 3.4\%$ were found in the SLB (Fig. 1b, e, p and s). In addition, cell aggregates of transplants that were located in the perilymphatic space were adjacent to those located in the SL (Fig. 1c and d). Within the SLB, the transplanted cells were located in the medial region, which faced the SV (Fig. 1e, p and s). BMSC-derived cells were also observed in other compartments of the cochleae: the sensory epithelium (Fig. 1f and g), the osseous spiral lamina (Fig. 1e and f) and the acoustic nerve (Fig. 1h).

Before transplantation, $74.2 \pm 17.6\%$ of the BMSCs expressed CD34 (Fig. 1i–k) and $3.5 \pm 2.0\%$ were immunoreactive for nestin (Fig. 1l–n). No immunoreactivity for the other markers used in this study was identified in the BMSCs before transplantation. Two weeks after transplantation into the cochleae, CD34-positive transplants were found (Fig. 1p–r); however, the expression ratio for CD34 in the BMSC-derived cells had significantly decreased to $7.3 \pm 8.3\%$ (Fig. 1o, $P=0.0003$). Immunoreactivity for nestin was still detected, but was significantly reduced to $0.9 \pm 0.8\%$ (Fig. 1o, $P=0.04$). Cx26 expression was detected in $4.7 \pm 2.7\%$ of the BMSC-derived cells that had settled in the cochleae (Fig. 1o, s–u). The difference in the ratio of Cx26 expression between before and after transplantation was significant at $P=0.02$. By contrast, immunoreactivity for E-cadherin and β-III-tubulin was not found in these cells.

Discussion

We hypothesized that BMSC transplantation could be utilized in three different strategies for inner ear treatment, restoration of missing cells, providing growth factors and delivering genes. These findings demonstrate that BMSCs can survive in various parts of the cochleae after injection into the perilymphatic space of cochleae, indicating possible use of BMSC transplantation for providing growth factors in the cochlea. These results, however, demonstrated significant decrease of the rate for CD34 expression in BMSC-derived cells in cochleae in comparison with that in BMSCs before transplantation, indicating maturation

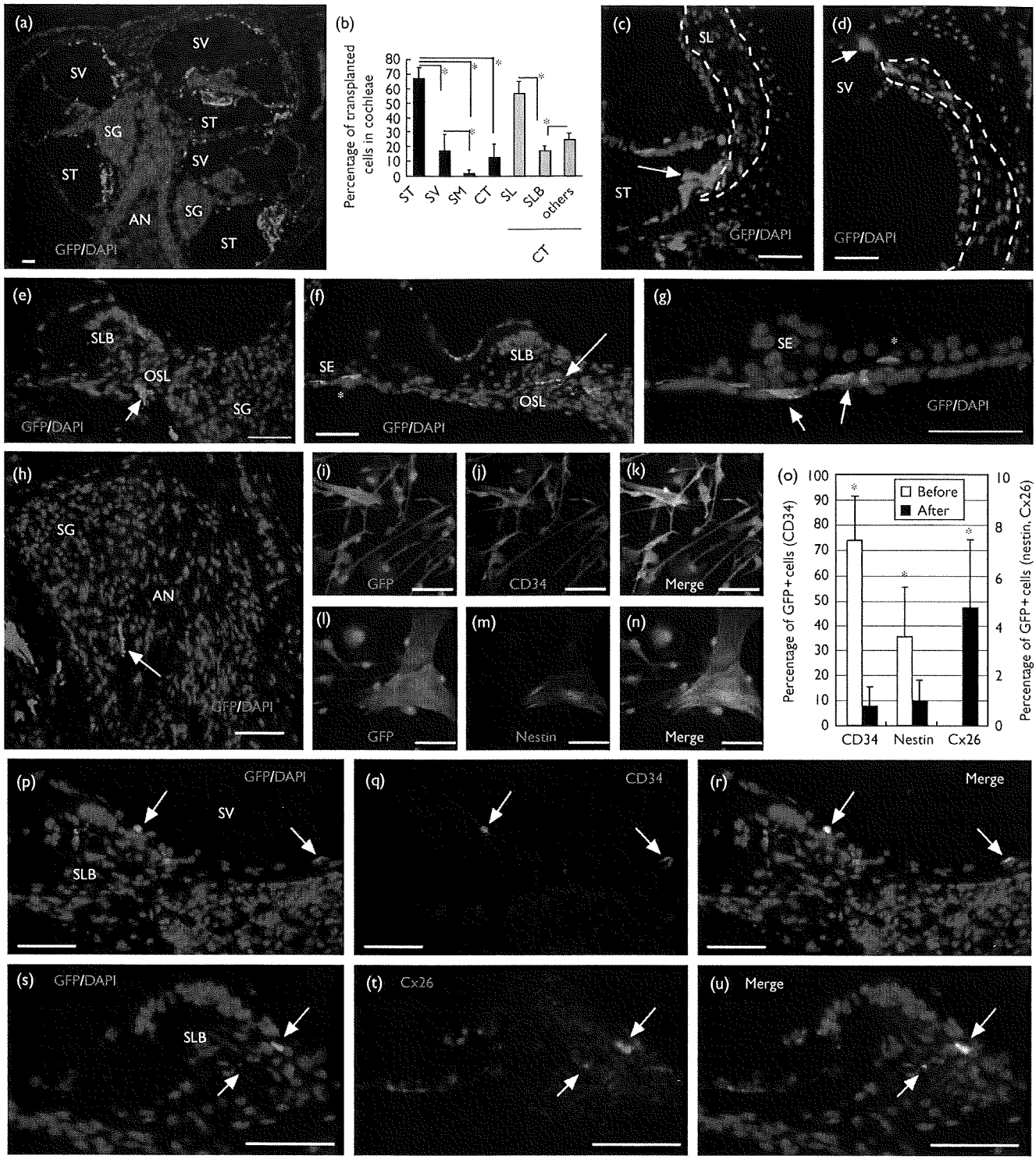

Fig. 1 Distribution of engrafted bone-marrow stromal cells in the cochlea and the expression of cell markers before and after transplantation. Transplanted cells expressing green fluorescent protein (GFP) were observed from the base to the apex of the cochleae, and were mainly located in the scala tympani (ST) and the scala vestibuli (SV) (a). Among the cochlear compartments, the transplanted cells were most frequently found in the ST (analysis of variance with the Scheffe's test, $^*P<0.05$ in b) and in cochlear tissue (CT), the spiral ligament (SL) is the site in which transplanted cells were most frequently observed (b). Some of the transplanted cells in the ST (arrow in c) or the SV (arrow in d) were located adjacent to the SL (indicated by the dotted lines in c, d) in which transplanted cells were found. Transplanted cells were also observed in the spiral limb (SLB) (e, p, s), the osseous spiral lamina (OSL) (arrow in e, f), the sensory epithelium (SE) (asterisk in f, g), the connective tissue beneath the SE (arrows in g) and the acoustic nerve (AN) (arrow in h). Before transplantation, the BMSCs expressed CD34 (i–k) and a few were positive for nestin expression (l–n). The ratio of CD34 or nestin expression was significantly reduced after transplantation (unpaired *t*-test, $^*P<0.05$ in o), and that of connexin26 (Cx26) expression was significantly increased after transplantation (o, the *y*-axis on the right side shows percentage for the CD34 ratio and the left for the ratio of nestin or Cx26). The transplanted cells that settled in the SV exhibited the expression of CD34 (arrows in p–r), and those in the SLB showed Cx26 expression (arrow in s–u). The scale bars represent 50 μm. Bars in b and o show standard deviations.

of BMSCs after transplantation. It is unclear whether BMSC-derived cells in the cochlea preserve the capability for secretion of growth factors displayed by BMSCs before transplantation [8]. Therefore, the potential of BMSC-derived cells in the cochlea for the secretion of growth factors should be examined to determine the ability of application of growth factors in the cochlea by BMSC transplantation.

Previously, we have demonstrated the delivery of a secreting protein to the inner ear by transplanting genetically manipulated fibroblasts without using virus vectors [7]. The fibroblasts were, however, distributed throughout the perilymphatic space of the cochlea and not within the cochlear tissues. These findings demonstrate the settlement of BMSC-derived cells within the cochlear tissues, particularly within the SL and SLB, after transplantation into the perilymphatic space of cochleae, suggesting the potential of BMSCs for migration into the SL and the SLB. These observed trends in the sites for BMSC migration indicate that the cells are suitable candidates for delivering genes in these regions, because delivery of cochlear constructive proteins may be required for the settlement of genetically manipulated cells in the regions in which encoded proteins should be expressed.

The gap junction network in the SL and the SLB has been suggested to play a crucial role in the maintenance of the endocochlear potential, which is necessary for hearing [13,14]. Our data demonstrate that some of the BMSC-derived cells that settled in the cochleae expressed Cx26, indicating the possible use of BMSC transplantation for restoration of the gap junction network in the cochlear connective tissues. The number of BMSC-derived cells expressing Cx26, however, may not be sufficient for the restoration of the gap-junction network. We should develop further strategies for increasing the number of BMSC-derived cells that settle within these regions to realize cochlear functional recovery by BMSC transplantation.

Immunohistochemical analyses in this study demonstrated no transdifferentiation of BMSCs into the neural or epithelial lineage after transplantation into the cochleae. In contrast to these findings, previous studies have demonstrated that BMSCs can differentiate into various types of cells including a neural lineage [15,16]. Naito *et al.* [17] have reported a differentiation of BMSCs into neurons after transplantation into the modiolus of chinchilla cochleae that had been damaged by aminoglycosides; however, the number of BMSC-derived cells expressing a neural marker is very limited. In this study, we identified the expression of nestin in BMSCs before and after transplantation, although the number is very limited. We therefore consider that neural induction of BMSCs and selection of neural progenitors from BMSC-derived cells before transplantation might be necessary to achieve the restoration of cochlear neurons through the transplantation of BMSCs.

Conclusion

In summary, our current findings demonstrate that BMSCs have the capability to survive in the cochlea and migrate into the cochlear tissues, which indicates possible use of BMSC transplantation as a strategy for the treatment of SNHL. Further studies are, however, necessary to realize the practical use of BMSC transplantation for the treatment of inner ears.

Acknowledgements

The authors thank Y. Nishiyama and R. Sadato for their technical assistance. This study was supported, in part, by a Grant-in-Aid for Scientific Research (B2, 16390488) from the Ministry of Education, Culture, Sports, Science and Technology of Japan, by a grant from the Takeda Science Foundation and by Higher Education Commission, Islamabad, Pakistan and Ministry of Science and Technology of Pakistan.

References

1. Tateya I, Nakagawa T, Iguchi F, Kim TS, Endo T, Yamada S, *et al.* Fate of neural stem cells grafted into injured inner ears of mice. *Neuroreport* 2003; **14**:1677–1681.
2. Izumikawa M, Minoda R, Kawamoto K, Abrashkin KA, Swiderski DL, Dolan DF, *et al.* Auditory hair cell replacement and hearing improvement by Atoh1 gene therapy in deaf mammals. *Nat Med* 2005; **11**:271–276.
3. Okano T, Nakagawa T, Endo T, Kim TS, Kita T, Tamura T, *et al.* Engraftment of embryonic stem cell-derived neurons into the cochlear modiolus. *Neuroreport* 2005; **16**:1919–1922.
4. Yagi M, Magal E, Sheng Z, Ang KA, Raphael Y. Hair cell protection from aminoglycoside ototoxicity by adenovirus-mediated overexpression of glial cell line-derived neurotrophic factor. *Hum Gene Ther* 1999; **10**: 813–823.
5. Chen X, Frisina RD, Bowers WJ, Frisina DR, Federoff HJ. HSV amplicon-mediated neurotrophin-3 expression protects murine spiral ganglion neurons from cisplatin-induced damage. *Mol Ther* 2001; **3**:958–963.
6. Hakuba N, Watabe K, Hyodo J, Ohashi T, Eto Y, Taniguchi M, *et al.* Adenovirus-mediated overexpression of a gene prevents hearing loss and progressive inner hair cell loss after transient cochlear ischemia in gerbils. *Gene Ther* 2003; **10**:426–433.
7. Okano T, Nakagawa T, Kita T, Endo T, Ito J. Cell-gene delivery of brain-derived neurotrophic factor to the mouse inner ear. *Mol Ther* 2006; **14**: 866–871.
8. Nagaya N, Kangawa K, Itoh T, Iwase T, Murakami S, Miyahara Y, *et al.* Transplantation of mesenchymal stem cells improves cardiac function in a rat model of dilated cardiomyopathy. *Circulation* 2005; **112**:1128–1135.
9. Oshima K, Shimamura M, Mizuno S, Tamai K, Doi K, Morishita R, *et al.* Intrathecal injection of HVJ-E containing HGF gene to cerebrospinal fluid can prevent and ameliorate hearing impairment in rats. *FASEB J* 2004; **18**:212–214.
10. Iwai K, Nakagawa T, Endo T, Matsuoka Y, Kita T, Kim TS, *et al.* Cochlear protection by local IGF-1 application using biodegradable hydrogel. *Laryngoscope* 2006; **116**:526–533.
11. Picciotti PM, Fetoni AR, Paludetti G, Wolf FI, Torsello A, Troiani D, *et al.* Vascular endothelial growth factor (VEGF) expression in noise-induced hearing loss. *Hear Res* 2006; **214**:76–83.
12. Okabe M, Ikawa M, Kominami K, Nakanishi T, Nishimune Y. 'Green mice' as a source of ubiquitous green cells. *FEBS Lett* 1997; **407**:313–319.
13. Xia A, Kikuchi T, Hozawa K, Katori Y, Takasaka T. Expression of connexin 26 and Na, K-ATPase in the developing mouse cochlear lateral wall: functional implications. *Brain Res* 1999; **846**:106–111.
14. Hirose K, Liberman MC. Lateral wall histopathology and endocochlear potential in the noise-damaged mouse cochlea. *J Assoc Res Otolaryngol* 2003; **4**:339–352.
15. Dezawa M, Hoshino M, Ide C. Treatment of neurodegenerative diseases using adult bone marrow stromal cell-derived neurons. *Expert Opin Biol Ther* 2005; **5**:427–435.
16. Lu J, Moochhala S, Moore XL, Ng KC, Tan MH, Lee LK, *et al.* Adult bone marrow cells differentiate into neural phenotypes and improve functional recovery in rats following traumatic brain injury. *Neurosci Lett* 2006; **398**:12–17.
17. Naito Y, Nakamura T, Nakagawa T, Iguchi F, Endo T, Fujino K, *et al.* Transplantation of bone marrow stromal cells into the cochlea of chinchillas. *Neuroreport* 2004; **15**:1–4.

BRAIN RESEARCH 1177 (2007) 47–58

available at www.sciencedirect.com

ScienceDirect

www.elsevier.com/locate/brainres

BRAIN RESEARCH

Research Report

Effects of heat stress on filamentous actin and prestin of outer hair cells in mice

Yoko Kitsunai[a,1], Naohiro Yoshida[b,1], Michio Murakoshi[a,1], Koji Iida[a], Shun Kumano[a], Toshimitsu Kobayashi[b], Hiroshi Wada[a,*]

[a]Department of Bioengineering and Robotics, Tohoku University, 6-6-01 Aoba-yama, Sendai 980-8579, Japan
[b]Department of Otolaryngology, Tohoku University Graduate School of Medicine, 1-1 Seiryo-machi, Sendai 980-8574, Japan

ARTICLE INFO

Article history:
Accepted 8 August 2007
Available online 16 August 2007

Keywords:
Heat stress
Outer hair cell
Filamentous actin
Prestin
Heat shock protein 27
Confocal laser scanning microscopy

ABSTRACT

When the ear is exposed to traumatic loud noise, outer hair cells (OHCs) are damaged and thus permanent hearing loss occurs. Recently, prior conditioning with heat stress has been reported to protect OHCs from traumatic noise exposure by increasing the stiffness of the OHC soma and has also been reported to enhance distortion product otoacoustic emissions [DPOAEs; Murakoshi, M., Yoshida, N., Kitsunai, Y., Iida, K., Kumano, S., Suzuki, T., Kobayashi, T., Wada, H., 2006. Effects of heat stress on Young's modulus of outer hair cells in mice. Brain Res. 1107, 121–130]. In the present study, to further investigate the heat stress-induced protective mechanism of hearing and such stress-induced DPOAE enhancement mechanism, the amount of filamentous actin (F-actin), which is concerned with cell stiffness, and the amount of prestin, which is concerned with the generation of DPOAEs, were examined in OHCs, with and without heat stress. Heat stress was found to increase the amount of F-actin 6–24 h after heat stress. The greatest increase in the amount of F-actin was observed at the cuticular plate where F-actin anchors the roots of the stereocilia to the cell body. Based on this result, the part of the stereocilia most reinforced and protected by heat stress was concluded to be the roots of the stereocilia. In contrast with F-actin, heat stress did not affect the amount of prestin.

1. Introduction

Outer hair cells (OHCs), located on the basilar membrane as a part of the organ of Corti in the cochlea, can change their length in response to changes in membrane potential, which is known as electromotility (Ashmore, 1987; Brownell et al., 1985; Kachar et al., 1986; Santos-Sacchi and Dilger, 1988). The force generated by this electromotility of OHCs amplifies the vibration of the basilar membrane, i.e., cochlear amplification, which enables the high sensitivity, wide dynamic range and sharp frequency selectivity of hearing in mammals.

When the ear is exposed to intense and/or prolonged sound, the organ of Corti and hair cells, especially the OHCs, are damaged, resulting in a permanent threshold shift (PTS). Recently, it has been reported that OHCs can be protected from traumatic noise exposure by prior sublethal conditioning such as nontraumatic sound exposure, heat stress, ischemia and physical restraint (Canlon et al., 1988; Yoshida et al., 1999; Yoshida and

* *Corresponding author.* Fax: +81 22 795 6939.
E-mail address: wada@cc.mech.tohoku.ac.jp (H. Wada).

Abbreviations: CLSM, confocal laser scanning microscopy; DPOAE, distortion product otoacoustic emissions; ECL, enhanced chemiluminescence; F-actin, filamentous actin; FITC, fluorescein isothiocyanate; HRP, horseradish peroxidase; HSP27, heat shock protein 27; OHC, outer hair cell; PTS, permanent threshold shift

[1] These authors contributed equally to this work.

0006-8993/$ – see front matter © 2007 Elsevier B.V. All rights reserved.
doi:10.1016/j.brainres.2007.08.019

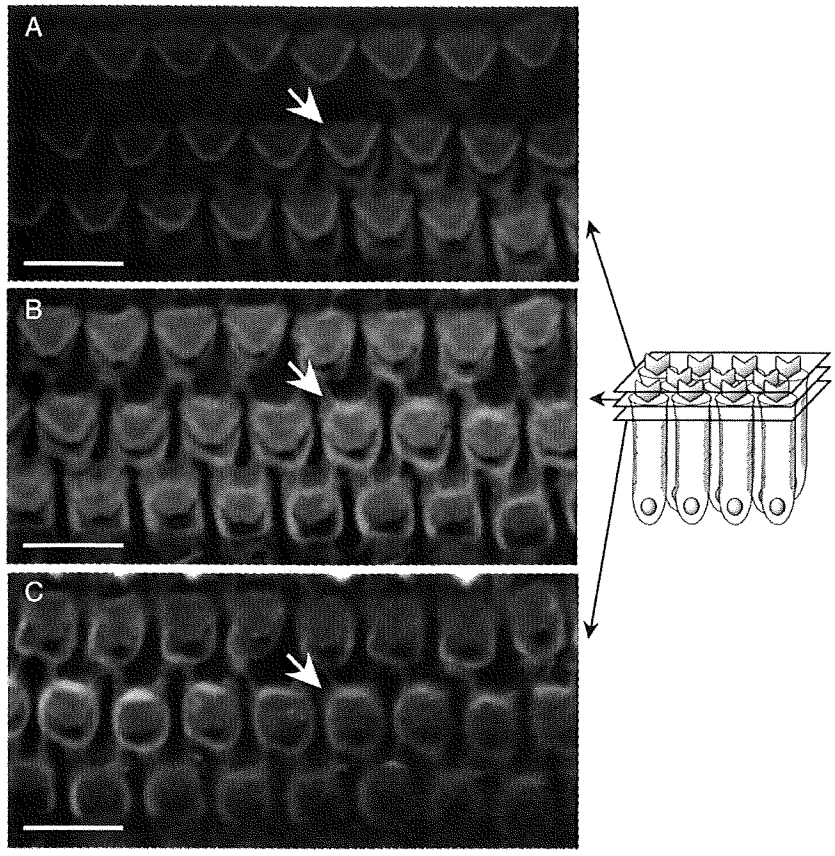

Fig. 1 – Fluorescence micrographs of the organ of Corti labeled with rhodamine–phalloidin in the normal mouse cochlea. The stereocilia, cuticular plate and lateral wall of the OHC were defined by referring to the OHC indicated by arrows. (A) Stereocilia (2 μm above the cuticular plate). (B) Cuticular plate. (C) Lateral wall (3 μm below the cuticular plate). Scale bars represent 10 μm.

Liberman, 2000; Wang and Liberman, 2002; Welch, 1992). Yoshida et al. (1999) reported that heat-stressed mice showed a reduction of PTS caused by subsequent intense sound exposure.

Although the mechanism of this protective effect remains unclear, one possibility is that modification of the OHC stiffness reduces the damage induced by traumatic exposure. Recently, heat stress has been found to increase the amount of filamentous actin (F-actin) in the OHC lateral wall with a consequent increase in wall stiffness (Murakoshi et al., 2006). Due to this increase in stiffness, intense noise causes less strain in OHCs, resulting in prevention of cell destruction.

However, to clarify the mechanism of heat stress-related hearing protection, investigation of only OHC lateral wall modification is insufficient because in many cases, noise-induced

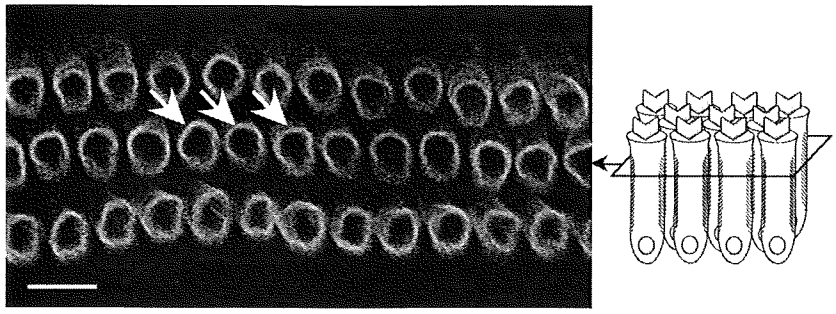

Fig. 2 – Fluorescence micrograph of the organ of Corti labeled with anti-prestin (C-16) primary antibody and FITC conjugated secondary antibody in the normal mouse cochlea. Because the surface of the organ of Corti is undulant, the z position of the cuticular plate differed from OHC to OHC. This micrograph was obtained at 2 μm below the cuticular plate of the OHCs which were indicated by arrows. Scale bar represents 10 μm.

hearing loss occurs due to the destruction of the roots of the OHC stereocilia (Liberman, 1987; Liberman and Beil, 1979), which are one of the most important structures for OHC function and the most mechanically vulnerable to sound exposure. However, the structural changes of the stereocilia and cuticular plate in which the stereocilia are anchored remain unclear.

Enhancement of distortion product otoacoustic emissions (DPOAEs), which reflects the activity of OHC electromotility, after heat stress was also observed by Murakoshi et al. (2006). These findings indicate the possibility that the amount of prestin increases after heat stress because prestin is a generator of the OHC electromotility and its expression has been reported to be concerned with the production of DPOAEs (Huang et al., 2005; Liberman et al., 2002; Zhu et al., 2006); however, it is unknown whether the amount of prestin increases after heat stress.

In the present study, therefore, animals were heat stressed by a previously proposed protocol, i.e., 15-min whole-body

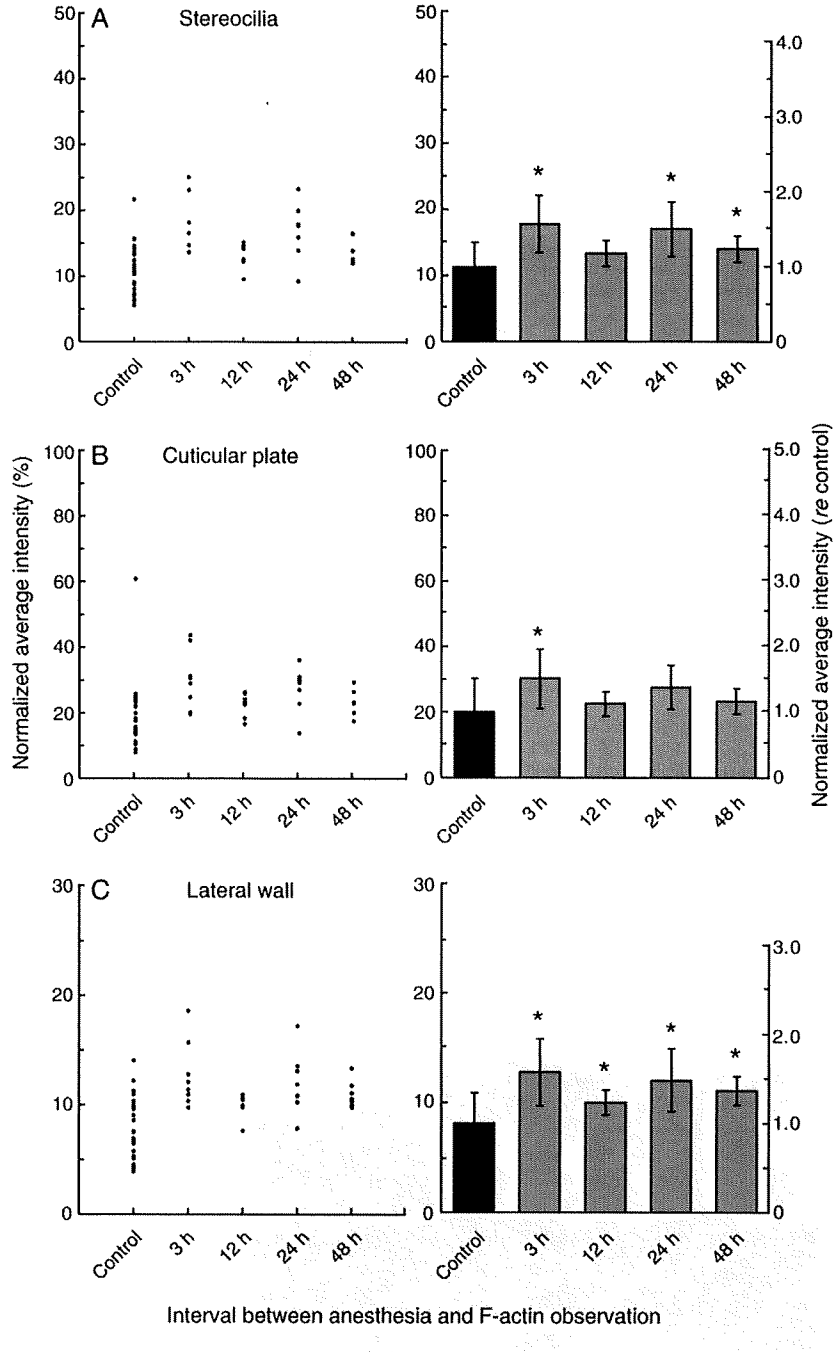

Fig. 3 – Intensity of F-actin labeling in the control group ($n=25$) and anesthesia only groups with 3-h ($n=8$), 12-h ($n=7$), 24-h ($n=8$) and 48-h ($n=7$) intervals. (A) Stereocilia. (B) Cuticular plate. (C) Lateral wall. In the left panels, each dot represents the normalized average intensity of F-actin labeling obtained from 16 OHCs in each organ of Corti. In the right panels, each bar represents the mean of the normalized average intensity of F-actin labeling. Asterisks indicate statistically significant differences between the control group and anesthesia only groups ($P<0.05$, Student's t-test).

heat stress (Yoshida et al., 1999), and heat stress-induced changes in the amount of F-actin, prestin and heat shock protein 27 (HSP27), which is a factor affecting the formation of F-actin, were investigated. The amount of F-actin was measured at several positions of OHCs, i.e., the stereocilia, cuticular plate and lateral wall of OHCs by confocal laser scanning microscopy (CLSM). The amount of prestin was investigated at the OHC lateral wall by CLSM. The amount of HSP27 within the cochlea was examined by Western blotting.

2. Results

2.1. *Distribution of F-actin and prestin in the mouse OHCs*

Fig. 1 shows fluorescence micrographs of the organ of Corti labeled with rhodamine–phalloidin in the normal mouse cochlea. The stereocilia, cuticular plate and lateral wall of the OHC, which were defined by referring to the OHC indicated

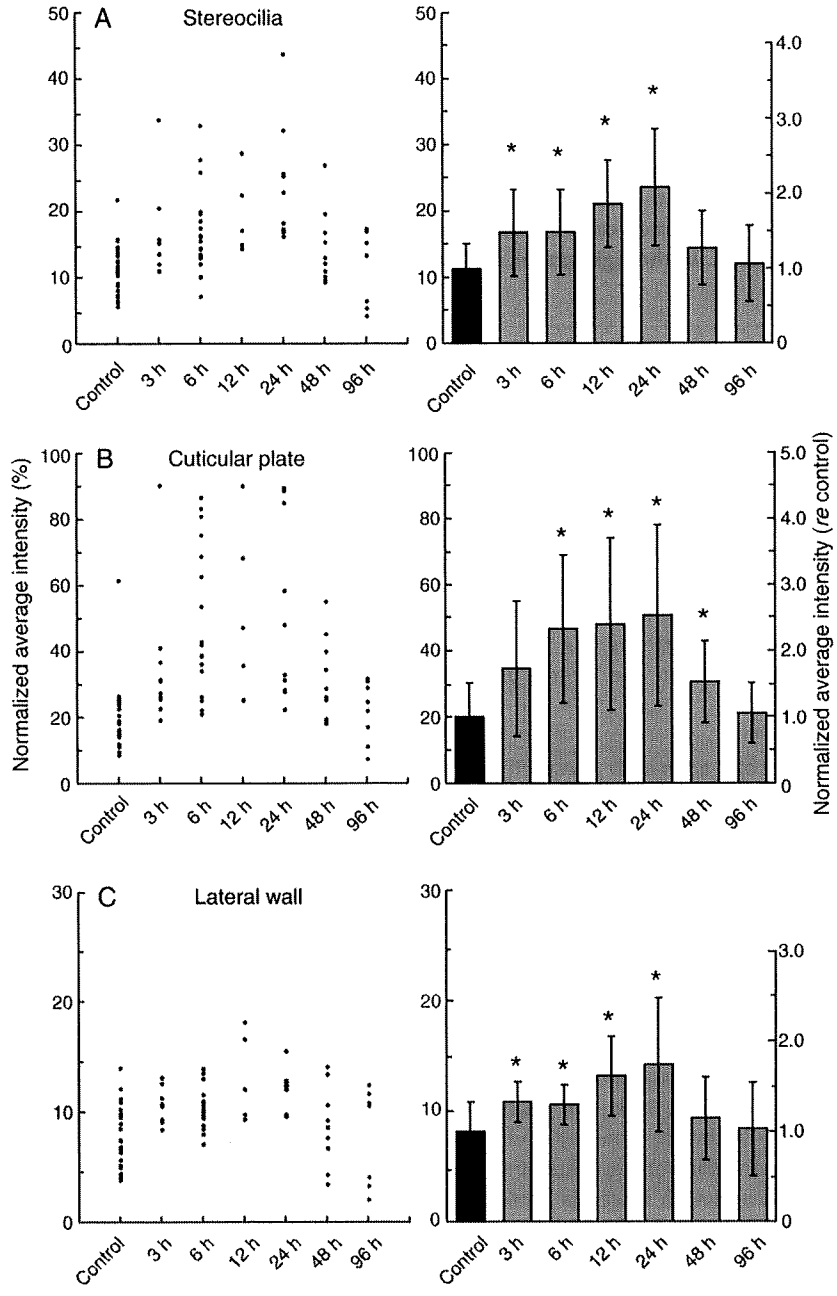

Fig. 4 – Intensity of F-actin labeling in the control group ($n=25$) and anesthesia+heat groups with 3-h ($n=10$), 6-h ($n=19$), 12-h ($n=6$), 24-h ($n=10$), 48-h ($n=10$) and 96-h ($n=8$) intervals. (A) Stereocilia. (B) Cuticular plate. (C) Lateral wall. In the left panels, each dot represents the normalized average intensity of F-actin labeling obtained from 16 OHCs in each organ of Corti. In the right panels, each bar represents the mean of the normalized average intensity of F-actin labeling. Asterisks indicate statistically significant differences between the control group and anesthesia+heat groups ($P<0.05$, Student's t-test).

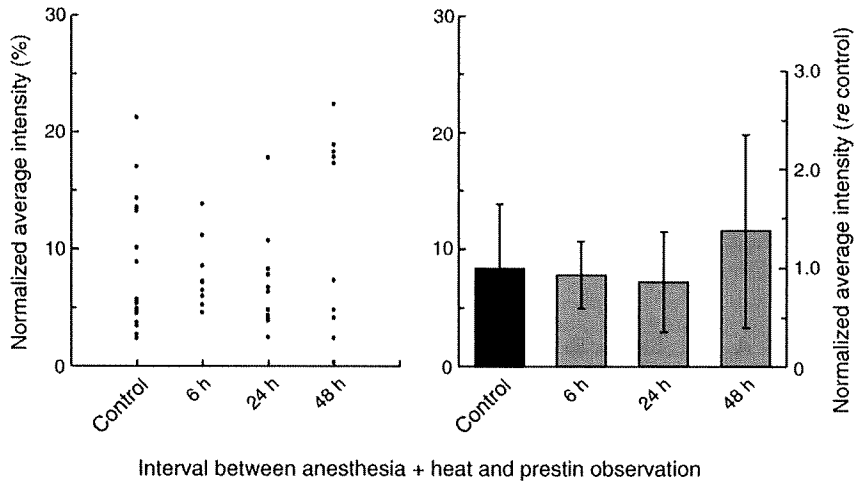

Fig. 5 – Intensity of prestin labeling in the control group ($n=18$) and anesthesia+heat groups with 6-h ($n=10$), 24-h ($n=11$) and 48-h ($n=10$) intervals. In the left panel, each dot represents the normalized average intensity of prestin labeling obtained from 9 OHCs in each organ of Corti. In the right panel, each bar represents the mean of the normalized average intensity of prestin labeling.

by arrows, are shown in Figs. 1A–C, respectively. As shown in these figures, rhodamine–phalloidin labeled the V-shaped stereocilia, cuticular plate and circumferential-ringed lateral wall of OHCs, indicating that F-actin is distributed at these positions.

Fig. 2 shows a fluorescence micrograph of the organ of Corti labeled with anti-prestin primary antibody and FITC conjugated secondary antibody. This micrograph was obtained at 2 μm below the cuticular plate of the OHCs indicated by arrows. The annular patterns can be clearly seen, indicating that prestin exists on the lateral plasma membrane of OHCs.

2.2. *Changes in the amount of F-actin after anesthetization*

Fig. 3 shows the intensity of F-actin labeling after anesthetization. The left panels show the normalized average intensities of F-actin labeling in the control and anesthesia only groups obtained at the stereocilia, cuticular plate and lateral wall, respectively. Dots represent the normalized average intensities in each organ of Corti. The right panels show the mean and standard deviation of the corresponding left panels.

As shown by the right panel of Fig. 3A, the mean of the normalized average intensities at the stereocilia increased 1.58-, 1.18-, 1.51- and 1.25-fold by 3 h, 12 h, 24 h and 48 h after anesthetization, respectively. Statistical analysis indicated significant differences between the control group and anesthesia only groups with 3-h, 24-h and 48-h intervals ($P<0.05$ by Student's *t*-test).

As shown by the right panel of Fig. 3B, the mean of the normalized average intensities at the cuticular plate increased 1.51-, 1.12-, 1.38- and 1.16-fold by 3 h, 12 h, 24 h and 48 h after anesthetization, respectively. Statistical analysis indicated a significant difference between the control group and anesthesia only group with a 3-h interval ($P<0.05$ by Student's *t*-test).

As shown by the right panel of Fig. 3C, the mean of the normalized average intensities at the lateral wall increased 1.58-, 1.23-, 1.48- and 1.37-fold by 3 h, 12 h, 24 h and 48 h after anesthetization, respectively. Statistical analysis indicated significant differences between the control group and anesthesia only groups with all intervals ($P<0.05$ by Student's *t*-test).

2.3. *Changes in the amount of F-actin after heat stress*

Fig. 4 shows the intensity of F-actin labeling after heat stress. The left panels show the normalized average intensities of F-actin labeling in the control and anesthesia+heat groups measured at the stereocilia, cuticular plate and lateral wall, respectively. The right panels show the mean and standard deviation of the corresponding left panels.

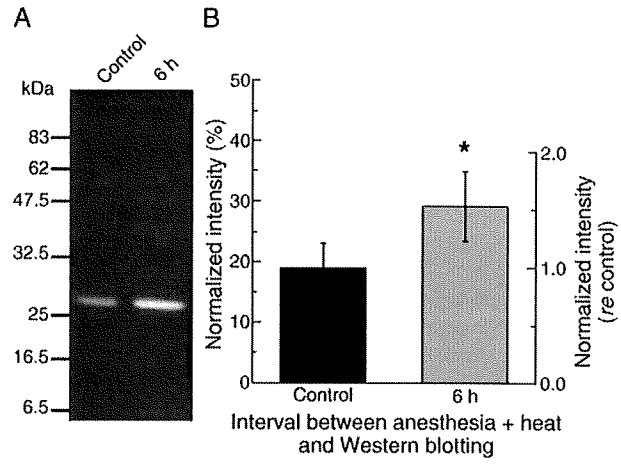

Fig. 6 – HSP27 expression within the cochlea in the control group and anesthesia+heat group with a 6-h interval. (A) An example of Western blotting. Bands were visible at around 27 kDa. (B) The mean of the normalized intensity of the HSP27 band in the control group ($n=14$) and the anesthesia+heat group with a 6-h interval ($n=14$). The asterisk indicates a statistically significant difference between the control group and anesthesia+heat group ($P<0.05$, Student's *t*-test).

As shown by the right panel of Fig. 4A, the mean of the normalized average intensities at the stereocilia increased 1.49-, 1.50-, 1.90- and 2.10-fold by 3 h, 6 h, 12 h and 24 h after heat stress, respectively, and then decreased and returned to the control level by 48–96 h after heat stress. Significant differences were found between the control group and anesthesia+heat groups with 3-h, 6-h, 12-h and 24-h intervals ($P<0.05$ by Student's t-test).

As shown by the right panel of Fig. 4B, the mean of the normalized average intensities at the cuticular plate increased 1.72-, 2.32-, 2.40- and 2.53-fold by 3 h, 6 h, 12 h and 24 h after heat stress, respectively, and then returned to the control level by 96 h after heat stress. Statistical analysis indicated significant differences between the control group and anesthesia+heat groups with 6-h, 12-h, 24-h and 48-h intervals ($P<0.05$ by Student's t-test).

As shown by the right panel of Fig. 4C, the mean of the normalized average intensities at the lateral wall increased 1.33-, 1.31-, 1.62- and 1.75-fold by 3 h, 6 h, 12 h and 24 h after heat stress, respectively, and then returned to the control level by 48–96 h after heat stress. Significant differences were found between the control group and anesthesia+heat groups with 3-h, 6-h, 12-h and 24-h intervals ($P<0.05$ by Student's t-test).

2.4. *Changes in the amount of prestin after heat stress*

The left panel of Fig. 5 shows the normalized average intensity of prestin labeling in the control and anesthesia+heat groups. The mean and standard deviation of the left panel of Fig. 5 are shown in the right panel of this figure. Significant differences were not found between the control and anesthesia+heat groups with any intervals ($P>0.05$ by Student's t-test).

2.5. *Changes in the amount of HSP27 after heat stress*

Fig. 6A shows an example of the result of HSP27 expression within the cochlea examined by Western blotting. In the present study, we used anti-HSP25 antibody to detect HSP27 in the mouse cochlear sample since anit-HSP25 antibody would combine with both HSP27 and HSP25 on a nitrocellulose membrane (see Section 4.4.2). Because the molecular weight of HSP25 and HSP27 is 25 kDa and 27 kDa, respectively, the bands would theoretically be visible at those positions. However, as shown in Fig. 6A, a band is visible at only around 27 kDa and there is no band at around 25 kDa. Therefore, the expression level of HSP25 is low; rather, HSP27 is dominantly expressed in the mouse cochlea.

Fig. 6B shows the mean and standard deviation of the normalized intensity of the HSP27 band. The intensity of this band increased 1.53-fold by 6 h after heat stress. A significant difference was found between the control and anesthesia+heat group ($P<0.05$ by Student's t-test).

3. Discussion

3.1. *Effects of anesthetization on the amount of F-actin*

The anesthetic drugs, ketamine and xylazine, used in this study have been reported to induce physical stress (Lei et al., 2001; Oren et al., 1987). Because various kinds of physical and psychological stress, such as ischemia and physical restraint, have been reported to have protective effects against traumatic exposure (Canlon et al., 1988; Yoshida et al., 1999; Yoshida and Liberman, 2000; Wang and Liberman, 2002; Welch, 1992), any stress can possibly modulate OHCs to reduce the damage they suffer due to traumatic exposure. Thus, it is necessary to investigate the effects of anesthetization on the amount of F-actin of OHCs before the effect of heat stress on it can be examined.

As shown by the right panels of Figs. 3A–C, the amount of F-actin in the stereocilia, cuticular plate and lateral wall increased after anesthetization. Thus, the effect of anesthesia on the amount of F-actin is not negligible. In contrast to F-actin, the amount of prestin did not change after heat stress with anesthetization (Fig. 5). Therefore, it is not necessary to investigate the amount of prestin after the treatment of anesthetization.

3.2. *Effect of heat stress on the amount of F-actin*

3.2.1. *Heat stress-induced increase in the amount of F-actin*

As shown by the left panels of Figs. 4A–C, interanimal variability of the increase in F-actin induced by heat stress was greater than that induced by anesthesia (Figs. 3A–C), indicating that in the anesthesia+heat groups, F-actin in some animals greatly increased due to heat stress, while in others, it was hardly affected by heat stress. Because there were animals which were hardly affected by heat stress, the mean value of the normalized average intensity of F-actin labeling in the anesthesia+heat groups was thought to be underestimated (Fig. 4, right panels). Hence, when comparing the effect of heat stress with that of anesthetization on the amount of F-actin, comparison of their mean values would cause an error. Therefore, we focused on the individual data shown in the left panels of Figs. 3 and 4 rather than on the mean values shown in the right panels. In the animals which were greatly affected by heat stress, the increase in the amount of F-actin was greater than the anesthesia-induced increase in F-actin. Based on these results, in the present study, it can be said that the increase in the amount of F-actin in the stereocilia, cuticular plate and lateral wall tended to be induced by heat stress rather than by anesthesia, although it depended on the animals.

3.2.2. *Mechanism of an increase in the amount of F-actin after heat stress*

In our previous study, only the effects of heat stress on F-actin at the lateral wall of OHCs were examined (Murakoshi et al., 2006). In the present study, we measured changes in the amount of F-actin at the stereocilia and the cuticular plate as well as at the lateral wall after heat stress because the stereocilia and cuticular plate are of great importance in the realization of OHC function, i.e., electromotility. As shown in Figs. 4A–C, the amount of F-actin increased at all measured positions of OHCs 6–24 h after heat stress and returned to the control level 48–96 h after such stress.

From this result, there is a possibility that some proteins responsible for the increase in the amount of F-actin were upregulated in OHCs due to heat stress. One possibility is HSP27 because it has been reported to be involved in actin formational activity (Lavoie et al., 1993) and its expression level has been reported to increase after whole-body heat stress (Leger

et al., 2000). Therefore, to investigate the mechanism responsible for the increase in the amount of F-actin after heat stress, change in the amount of HSP27 due to such stress was examined by Western blotting. As shown in Fig. 6B, the amount of HSP27 increased 1.53-fold by 6 h after heat stress. This increase may induce actin polymerization, resulting in the increase in the amount of F-actin. Other than HSP27, Rho protein family GTPases have also been reported to contribute to the increase in the amount of F-actin (Schwartz, 2004). Their activities may also induce the increase in F-actin after heat stress.

In a previous study, it was reported that actin filaments of the mature stereocilia are continuously being turned over and that the entire core of the stereocilium is renewed every 48 h (Schneider et al., 2002). The time course of this 48-h renewal process of the stereocilia is consistent with that of the heat stress-induced change in the amount of F-actin in OHCs reported in the present study. This congruence of time courses implies that the increase in the amount of F-actin begun by 3 h after heat stress at the stereocilia, possibly induced by regulation of HSP in OHCs, was regulated to return to the control level by 48 h after stress due to this turnover process. However, the exact mechanism of heat stress-induced changes in the amount of F-actin is still controversial.

Although the amount of F-actin increased at all measured positions of OHCs after heat stress, the levels of such increase at the stereocilia and the cuticular plate were greater than that at the lateral wall. The greatest increase in the amount of F-actin was observed at the cuticular plate; that is, the amount of F-actin increased 2.32-, 2.40- and 2.53-fold by 6 h, 12 h and 24 h after heat stress, respectively (Fig. 4B). The mechanisms that resulted in these different degrees of increase from position to position in this study are unclear. It is speculated that this phenomenon may be concerned with the relationship between F-actin formation and endocytotic activity as the formation of the actin filament has been reported to require such activity (Gottlieb et al., 1993). Additionally, Griesinger et al. (2004) reported that endocytosis of OHCs was the most prominent at the cuticular plate. Based on these reports, because of the active endocytosis at the cuticular plate, the formation of actin filaments may be accelerated at the cuticular plate after heat stress, resulting in the great increase in the amount of F-actin there. The distribution of the actin isoform was reported to differ from position to position in OHCs. Furness et al. (2005) demonstrated that β- and γ-actin colocalized at the stereocilia and cuticular plate while only γ-actin existed at the lateral wall, and that the rootlet was mainly composed of β-actin. Although it is unclear if F-actin formation activity differs between β-actin and γ-actin, the possibility that these differences may be concerned with the different levels of increase of F-actin in OHCs cannot be ruled out.

3.2.3. *Protective effects of heat stress on hearing*

F-actin has been reported to contribute to the stiffness of the cells. As reported by An et al. (2002) and Laurent et al. (2003), the stiffness of the cells increased when the amount of F-actin increased while it decreased when the amount of F-actin decreased. Those reports thus indicate that the increase in the amount of F-actin induced an increase in cell stiffness. Hence, in the present study, the stereocilia, cuticular plate and lateral wall of OHCs were thought to be stiffened by heat stress. According to the protective mechanism of heat stress that we previously proposed (Murakoshi et al., 2006), mammalian OHCs would experience less strain when they are exposed to loud noise due to increased stiffness of their lateral wall, resulting in protection of hearing from traumatic noise exposure. Based on this mechanism, the increased stiffness of the stereocilia and cuticular plate also probably contribute to this protective effect.

Actin filament in the cuticular plate tightly anchors the roots of the stereocilia to the cell body. The roots of the stereocilia are very vulnerable and the stereocilia are at a risk of being broken off from their roots (Liberman, 1987). This vulnerability of the roots of the stereocilia can be explained by considering a simple equivalent mechanical model in which a stereocilium is expressed as a homogeneous cylindrical cantilever beam which is fixed at the cuticular plate, as shown in Fig. 7. When the top of the stereocilium is subjected to shear force from the tectorial membrane, $F_{\text{Tectorial membrane}}$, the stereocilium bends, as shown by the dashed line in Fig. 7. The bending stress, σ, is given by

$$\sigma = \frac{My}{I} = \frac{F(l-x)y}{I}, \tag{1}$$

where M is the bending moment, l is the length of the stereocilium, x is the distance from the cuticular plate, y is the perpendicular distance from the neutral axis, i.e., the x axis, and I is the moment of inertia of the cross-sectional area of the stereocilium, which is given by

$$I = \frac{\pi d^4}{64}, \tag{2}$$

where d is the diameter of the stereocilium. Derived from Eqs. (1) and (2), the bending stress becomes the greatest at $x=0$ and $y=\pm d/2$, i.e., at the circumference of the root of the stereocilium. Therefore, when animals are overexposed to intense noise, the damage to the stereocilia is the greatest at their roots and they may break off from their roots. Based on these considerations, it is reasonable to conclude that the phenomenon of the increased amount of F-actin being the greatest at the cuticular plate protects the roots of the stereocilia and thus maintains the normal function of OHCs following traumatic noise exposure.

The left panels of Figs. 4A–C indicate that F-actin in some animals greatly increased due to heat stress while F-actin in others was hardly affected by heat stress. However, most heat-stressed animals showed a reduction of PTS after heat stress (Yoshida et al., 1999). This incongruity suggests that there may be factors other than F-actin which increase the stiffness of OHCs and also suggests the presence of factors which prevent OHC apoptosis, oxidative stress, etc., induced by traumatic exposure other than the above-mentioned increase in the stiffness of OHCs.

3.3. *Effects of heat stress on the amount of prestin*

In previous studies, the changes in the amount of prestin in OHCs after certain treatments have been examined. Weber et al. (2002) reported that the expression level of prestin was decreased by the administration of an antithyroid drug. On the other hand, Zhu et al. (2006) reported that its expression level was increased by the administration of salicylate. Chen (2006) also reported that prestin gene expression was increased by

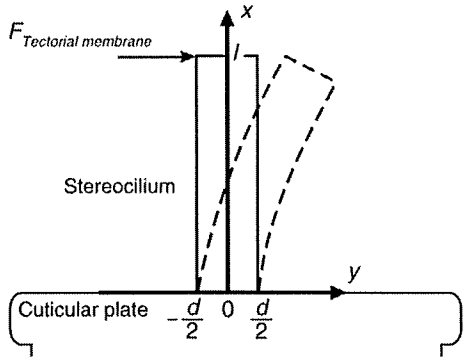

Fig. 7 – Mechanical model of the stereocilium. The stereocilium is expressed as a cantilever beam *l* in length and *d* in diameter, which is fixed at the cuticular plate. When the shear force, $F_{Tectorial\ membrane}$, between the tectorial membrane and reticular lamina is applied to the top of the stereocilium, the stereocilium bends as shown by the dashed line. Bending stress then occurs in the stereocilium, which is dependent on the distance, *x*, from the cuticular plate and the perpendicular distance, *y*, from the neutral axis, i.e., the *x* axis. The bending stress becomes the largest at $x=0$ and $y=\pm d/2$, i.e., at the circumference of the root of the stereocilium.

traumatic noise exposure. These findings indicate that the expression level of prestin may possibly be altered by external treatment.

In our previous study, DPOAE amplitude was found to be enhanced with statistical significance after heat stress (Murakoshi et al., 2006). DPOAE amplitude has been reported to be concerned with the amount of prestin. In a report on prestin knockout mice, DPOAE thresholds of homozygous mice (−/−), which did not express the prestin gene and protein, were higher than those of wild type mice (Liberman et al., 2002). In addition, 2-week administration of salicylate in guinea pigs has been reported to enhance DPOAE amplitude (Huang et al., 2005) as well as to enhance prestin mRNA expression (Zhu et al., 2006), suggesting that the high level expression of prestin induced by salicylate results in the enhancement of DPOAE amplitude. These results indicate that there is a possibility that the amount of prestin in OHCs increases after heat stress. However, in the present study, we found that the amount of prestin did not change after heat stress. Thus, the DPOAE enhancement demonstrated in our previous study is thought to be induced by a prestin-independent pathway. Instead, this enhancement is induced by the increase in OHC stiffness, as reported in our previous study (Murakoshi et al., 2006).

4. Experimental procedures

4.1. *Experimental groups and design*

The care and use of the animals in this study were approved by the Institutional Animal Care and Use Committee of Tohoku University, Sendai, Japan.

CBA/JNCrj strain male mice, aged 10–12 weeks (25–30 g), were used. Both left and right cochleae were used as samples, that is, two samples could be extracted from one experimental animal. Sample number, *n*, represents the number of cochleae examined. As shown in Fig. 8, animals were divided into three groups, i.e., a control group, an anesthesia only group and an anesthesia+heat group. Animals in the control group, which were used to clarify the normal amount of F-actin ($n=25$), prestin ($n=18$) and HSP27 ($n=14$) in OHCs of 10- to 12-week-old CBA/JNCrj mice, were not exposed to any stress. In the anesthesia only group, the animals were anesthetized 3 h ($n=8$), 12 h ($n=7$), 24 h ($n=8$) and 48 h ($n=7$) before F-actin labeling and CLSM observation. This group was established to differentiate the effects of heat stress on the amount of F-actin from those of anesthesia. The anesthesia+heat group consisted of three subgroups, that is, the animals for F-actin investigation, those for prestin investigation and those for HSP27 investigation. In the first group, animals were anesthetized and heat stressed 3 h ($n=10$), 6 h ($n=19$), 12 h ($n=6$), 24 h ($n=10$), 48 h ($n=10$) and 96 h ($n=8$) before F-actin labeling and CLSM observation. In the second group, animals were anesthetized and heat stressed 6 h ($n=10$), 24 h ($n=11$) and 48 h ($n=10$) before prestin labeling and CLSM observation. In the third group, animals were anesthetized and heat stressed 6 h ($n=14$) before Western blotting.

4.2. *Anesthesia and heat stress*

4.2.1. *Anesthesia only*

Animals were anesthetized with ketamine (60 mg/kg, i.p.) and xylazine (6 mg/kg, i.p.). After injection, they were placed on a heating pad maintained at 37 °C and were left on the pad before they fully recovered from the anesthesia (approximately 1 h). The rectal temperature of dormant animals was monitored by using a rectal thermometer and maintained at 36–37 °C. After recovery from anesthesia, the animals were returned to the animal care facility.

4.2.2. *Anesthesia+heat stress*

The animals were heat stressed as described previously (Yoshida et al., 1999; Murakoshi et al., 2006). They were anesthetized with ketamine (60 mg/kg, i.p.) and xylazine (6 mg/kg, i.p.). Once they were deeply anesthetized (approximately 10 min later), they were placed in an aluminum boat floating in a hot water bath maintained at 47.5 °C. To avoid direct effects of heat from the bottom of the boat, the animal's head was placed on a gauze pad. The rectal temperature was controlled so as to rise at an average rate of 0.6 °C/min. After it reached 41.5 °C, it was maintained at that temperature for 15 min. The animals were then transferred from the boat to the heating pad to fully recover from the anesthesia before being returned to the animal care facility.

4.3. *Protein expression analysis by CLSM*

4.3.1. *Cell preparation*

4.3.1.1. *Cochlear extraction and fixation.* Animals were anesthetized with diethylether and subsequently decapitated. Both left and right bullae were immediately removed and transferred to Petri dishes containing tissue culture medium (Leibovitz's L-15, Invitrogen, Carlsbad, CA) and the cochleae were then exposed with tweezers. Under a dissection microscope, 4%

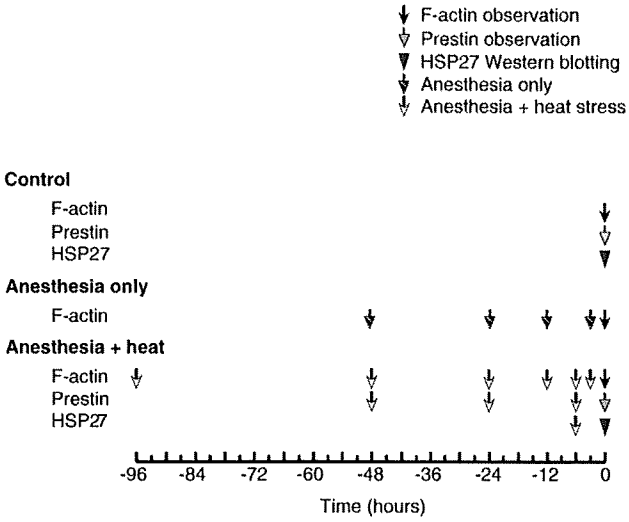

Fig. 8 – Experimental design. Experimental mice were divided into three groups, i.e., a control group, an anesthesia only group and an anesthesia+heat group. There were three subgroups of mice in the control group, i.e., the animals for F-actin investigation (n=25), those for prestin investigation (n=18) and those for HSP27 investigation (n=14). Their F-actin, prestin and HSP27 were observed without exposure to any stress. Mice in the anesthesia only groups were anesthetized 3 h (n=8), 12 h (n=7), 24 h (n=8) and 48 h (n=7) before F-actin observation. There were three subgroups of mice in the anesthesia+heat groups, i.e., the animals for F-actin investigation, those for prestin investigation and those for HSP27 investigation. In the first group, animals were anesthetized and heat stressed 3 h (n=10), 6 h (n=19), 12 h (n=6), 24 h (n=10), 48 h (n=10) and 96 h (n=8) before F-actin labeling and CLSM observation. In the second group, animals were anesthetized and heat stressed 6 h (n=10), 24 h (n=11) and 48 h (n=10) before prestin labeling and CLSM observation. In the third group, animals were anesthetized and heat stressed 6 h (n=14) before Western blotting.

paraformaldehyde in 0.1 M phosphate buffer adjusted to pH 7.4 (Wako, Osaka, Japan) was gently perfused into the cochlea through the round window with a fine pipette. Since the fixative penetrates the cochlear duct in accordance with concentration gradient, no exit hole was made in this study. The entire cochleae were then immersed in the same fixative for 1 h.

For comparison between the control group and anesthesia+heat groups, and between the control group and anesthesia only groups, the specimens of all groups should be prepared under the same conditions. For this reason, some specimens of the control group and the anesthesia+heat groups, and some specimens of the control group and anesthesia only groups were simultaneously prepared in an experimental chamber by the same experimenter. In addition, the experimenter was blind to the groups to which the specimens belonged until all data acquisition had been completed.

4.3.1.2. *F-actin labeling.* After the cochlea had been fixed for 1 h, it was dissected and the apical turn of the organ of Corti was removed and kept in the same fixative for 30 min. The specimens were immersed in 0.5% Triton X-100 (ICN Biomedicals, Irvine, CA) for 30 min, washed with PBS, immersed in Block Ace (Dainippon pharmaceutical, Osaka, Japan) for 1 h and rinsed in PBS. The specimens were then stained with 0.3 μM rhodamine–phalloidin (Sigma-Aldrich, St. Louis, MO) for 3 h. These procedures were performed at room temperature.

4.3.1.3. *Prestin labeling.* After 1-h fixation, the cochleae were washed in 10 μM glycine in PBS four times and dehydrated through a graded series of ethanol concentrations (30%, 50%, 70% and 100%) each for 15 min. The cochleae were dissected in 100% ethanol and the modiolus was exposed. The specimens were then immersed in 0.5% Triton X-100. The apical turn of the organ of Corti was then removed from the modiolus in this detergent and kept there for 30 min. Nonspecific background staining was blocked by incubation in blocking solution (5% donkey serum in Block Ace) for 2 h. The specimens were then incubated in 4 μg/ml of goat anti-prestin (C-16) antibody (Santa Cruz Biotechnology, Santa Cruz, CA) in the blocking solution for 12 h at 4 °C. After the specimens had been rinsed with PBS three times, they were incubated in 4 μg/ml of fluorescein isothiocyanate (FITC) conjugated donkey anti-goat IgG (Santa Cruz Biotechnology) dissolved in 5% donkey serum in PBS for 2 h at room temperature. To determine the position of an OHC, 270 nM rhodamine–phalloidin was also used to stain F-actin in the specimens. These procedures were performed at room temperature.

4.3.2. *CLSM*

4.3.2.1. *CLSM observation.* The specimens were placed on glass-bottomed dishes (MatTek, Ashland, MA) and immobilized with coverslips (Matsunami, Osaka, Japan). They were observed by CLSM (FV500, Olympus, Tokyo, Japan) with a 60× oil immersion objective. Gain and sensitivity of photomultiplier, laser power, exposure time and other parameters were set to be the same in every experiment.

Schemata of fluorescence micrograph acquisition for the F-actin observation and prestin observation are shown in Figs. 9A and B, respectively. Because fluorescence decay of FITC is faster than that of rhodamine, the sample labeled with FITC for prestin observation could not sustain as long an exposure time as the sample labeled with rhodamine for F-actin observation. Therefore, for prestin observation, 32–35 sheets of serial fluorescence micrographs were obtained from the top of the stereocilia to the bottom of the soma with intervals of 0.5 μm along the z axis, over a period of 50 s. For F-actin observation, 80–90 sheets of serial fluorescence micrographs were obtained from the top of the stereocilia to the bottom of the soma with intervals of 0.2 μm along the z axis, over a period of 500 s. Because the specimens were observed under the same conditions, the fluorescence of each substance decayed at the same speed. Hence, although the fluorescence decay occurred while micrographs were being acquired, the intensities in each group could be compared.

4.3.2.2. *Intensity analysis.* In the fluorescence micrographs, each pixel has an intensity value ranging from 0 (dark) to 4095 (light). For F-actin observation, circular analytic regions (ϕ 8 μm) were defined so that an OHC was located in each

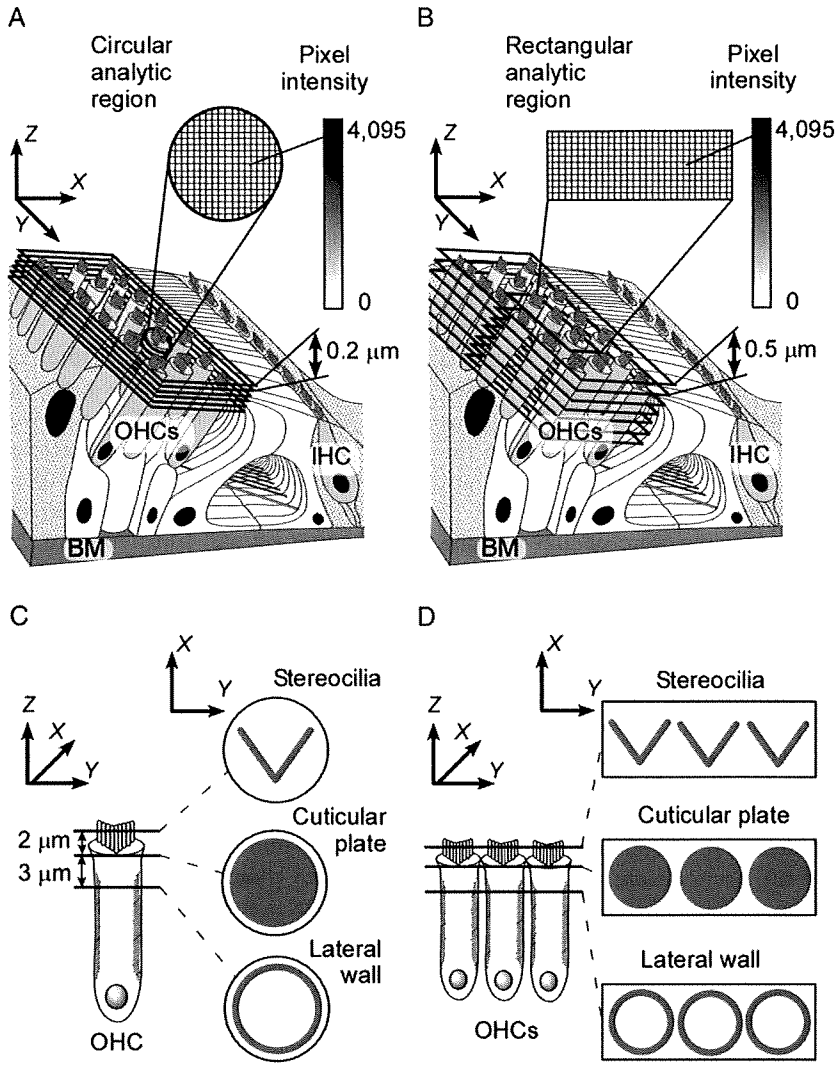

Fig. 9 – CLSM observation. (A) Acquisition of the fluorescence micrographs of the organ of Corti for F-actin investigation. Fluorescence micrographs were obtained from the top of the stereocilia to the bottom of the soma with intervals of 0.2 μm. In the micrograph, each pixel has an intensity value ranging from 0 (dark) to 4095 (light). Circular analytic regions (φ 8 μm) were defined so that an OHC was located in the center of each region. (B) Acquisition of the fluorescence micrograph of the organ of Corti for prestin investigation. Fluorescence micrographs were obtained from the top of the stereocilia to the bottom of the soma with intervals of 0.5 μm. Rectangular analytic regions (22.35×9.60 μm) were defined so that 3 OHCs were located in each region. (C, D) Definition of the position of the OHC, i.e., the stereocilia, cuticular plate and lateral wall. The position of OHCs was defined using the intensity of F-actin labeling. The intensity of F-actin labeling obtained from the cuticular plate is greater than that obtained from the stereocilia or lateral wall because the area occupied by the cuticular plate in the circular and rectangular analytic regions is larger than that occupied by the stereocilia (V shape) or lateral wall (circumference). Thus, the position where the greatest intensity of F-actin labeling was obtained was defined as the cuticular plate. The position 2 μm above and that 3 μm below the cuticular plate were referred to as the stereocilia and lateral wall, respectively. BM, basilar membrane; IHC, inner hair cell; OHC, outer hair cell.

region. The summation of the intensity of rhodamine in each pixel within a circular analytic region was defined as the intensity of F-actin labeling in the OHC (Fig. 9A). For prestin observation, rectangular analytic regions (22.35×9.60 μm) were defined so that 3 OHCs were located in each region. The summation of the intensity of rhodamine and that of FITC in each pixel within a rectangular analytic region was defined as the intensity of F-actin labeling and prestin labeling in the 3 OHCs, respectively (Fig. 9B). The difference in the analytic regions between F-actin and prestin observations was due to the difference in the length of the OHCs analyzed. For F-actin observation and prestin observation, intensities of the OHC lateral wall were analyzed up to 3 μm and up to 7 μm below the cuticular plate, respectively. A larger region along the OHC lateral wall was analyzed for prestin observation. As OHCs curved with distance from the cuticular plate, if the circular analytic region had been applied to prestin observation, the object OHC would have protruded from the analytic region or some OHCs adjacent to the object OHC would have been involved in the analytic region. To reduce the measurement